Geochemistry 85 (2025) 126285

Contents lists available at ScienceDirect

Geochemistry

journal homepage: www.elsevier.com/locate/chemer

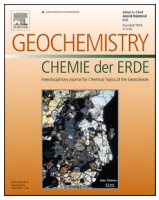

Polymetallic interactions of Zn-Pb-Cu in blue/green-colored speleothems from Malaval Cave (France)

Martin Vlieghe [a,*], Gaëtan Rochez [a], Stéphane Pire-Stevenne [b], Alexandre Felten [c,d], Marie Dechamps [c], Sébastien R. Mouchet [a,c,e], Francesca Cecchet [c], Olivier Bruguier [f], Jean-Louis Galéra [g], Gipsi Lima-Mendez [h], Marc Llirós Dupré [i], Johan Yans [a,*]

[a] Institute of Life, Earth and Environment, University of Namur, Namur, Belgium
[b] Groupe de Recherches et Photographie en Spéléologie, Namur, Belgium
[c] Namur Institute of Structured Matter, University of Namur, Namur, Belgium
[d] Synthesis, Irradiation & Analysis of Materials (SIAM) Technological Platform, University of Namur, Namur, Belgium
[e] School of Physics, University of Exeter, Exeter, UK
[f] Géosciences Montpellier, UMR5243, CNRS & Université de Montpellier, Montpellier, France
[g] Association Malaval, Ispagnac, Lozère, France
[h] Namur Research Institute of Life Sciences, Biology Department, University of Namur, Namur, Belgium
[i] Biosciences Department, Faculty of Sciences, Technology and Engineering, University of Vic, Vic, Catalonia, Spain

ARTICLE INFO

Handling Editor: Martin Dietzel

Keywords:
Speleothem
Coloration
Polymetallic
Weathering
Heavy metals

ABSTRACT

Speleothems rarely exhibit stunning colors such as red, yellow, green, or blue. The colorations are often linked to elevated heavy metal ion concentration in the drip water and thus to a metal source/pollution in the catchment area. Here the blue-green speleothems coloration in Malaval Cave (Lozère, France) is characterized by a wide panel of optical, mineralogical and geochemical techniques. These techniques were applied on several small blue or white stalactites and a larger greenish stalactite. The speleothems are mostly composed of aragonite and contain variable amounts of Zn, Cu and Pb, which cause the colorations. Zn and Cu are mostly present in substitution in the aragonite and Cu^{2+} is the main cause of the blue coloration. Zn is also found in small amorphous gel particles, containing minor amounts of Mg, Cu and Si. These phases are responsible for microscopical scale variations in the blue coloration. Pb is present as Pb^{2+} ions in substitution within the aragonite, creating a saturated blue-to-greenish coloration. This coloration may depend on the Pb/Zn ratio due to metallic interaction. Pb, Zn and Cu ratios indicate that Pb likely deposited from distinct fluids and at a different timing than Cu and Zn. All three metals likely originate from the leaching of Pb—Zn ores in the Jurassic formations surrounding the cave.

1. Introduction

Karstic caves consist of voids created in geological formations by dissolution of the carbonaceous host rock. They usually contain speleothems (namely stalactites and stalagmites), which are secondary mineral structures formed by the dissolution and recrystallization of carbonates from the host rock. As these structures are most often composed of calcite or aragonite, they are naturally white, but some can exhibit unusual colorations, such as red, yellow, green, black or blue. Studying these colorations is important, because they can be due to the presence of heavy metals or other pollutants and can thus be a good indicator of environmental pollution.

Recent studies in karstic systems mainly focus on past paleoclimate and environmental changes (Blyth et al., 2013; Fairchild et al., 2006) and on associated microbial activity (Maciejewska et al., 2015; Tisato et al., 2015) (see review in Hershey and Barton (2018)). Studies about the genesis of colored speleothems remain very scarce (White, 2019, 1997). Some examples are i) amberine speleothems in the Spanish El Soplao cave, associated with fossil organic matter (Gázquez et al., 2012), ii) blue speleothems at Cliefden (Australia), which is proposed to be related to minor concentrations of Cu, Cr and Ni (Turner, 2002), iii) variously colored speleothems in the Spanish Basajaún Etxea Cave,

* Corresponding authors.
E-mail addresses: martin.vlieghe@unamur.be (M. Vlieghe), johan.yans@unamur.be (J. Yans).

https://doi.org/10.1016/j.chemer.2025.126285
Received 25 October 2024; Received in revised form 17 March 2025; Accepted 18 March 2025
Available online 20 March 2025

partly explained by the diagenesis of aragonite/calcite speleothems (Martín-García et al., 2014), and iv) green-colored speleothems in the Aven du Mont Marcou (Southern France), which are due to the presence of a green Ni-bearing phyllosilicate – nepouite – within the aragonite and calcite speleothems (Vlieghe et al., 2023). A review of the topic of trace elements in speleothems highlighted that potential colorations induced by trace elements have been poorly studied (Verheyden, 2004).

In this article, we propose a detailed study about the origin of the blue-to-greenish speleothem coloration in Malaval Cave (Cevennes Massif, Lozère, France) (Fig. 1a-b), using a wide variety of techniques, such as X-ray Diffraction (XRD) and Raman micro-spectroscopy, Scanning Electron Microscopy and Energy Dispersive X-ray Spectroscopy (SEM/EDS), Inductively Coupled Plasma-Mass Spectrometry (ICP-MS) in solution and Laser Ablation Inductively Coupled Plasma-Mass Spectrometry (LA-ICP-MS), Time of Flight Secondary Ion Mass Spectrometry (ToF-SIMS), X-ray Photoelectron Spectroscopy (XPS), as well as optical measurements allowing colorimetric quantification. These analyses shed light on the precise causes of the coloration and on the origin of coloring elements of speleothems in caves. They also give information about the spatial distribution of the metallic contaminations, giving insights into the timing and precipitation conditions of the metals.

2. Geological context

Malaval Cave is located in the Lozère Department (France), about 9 km NE of Florac in the locality “Les Bondons”. The cave lies in a sedimentary structure called Avant-Causses, near two major geological structures, namely the Cevennes Massif and the Grands Causses (Fig. 2). The Cevennes Massif is mainly composed of Ordovician epimetamorphic schists, as well as a large Carboniferous granite massif. This granite constitutes the westernmost part of the Mont Lozère. The Grands Causses comprise a nearly complete subhorizontal series of Jurassic marine sediments, largely dominated by limestone and dolostone formations (Faure et al., 2001; Gèze et al., 1980). These sediments were impacted by mineralizing fluids originating from the underlying magmatic chamber during the Jurassic period, which created extensive Pb-Zn-(Ag) deposits mostly localized in the Hettangian sediments (Baron et al., 2006; Bouladon, 1960; Ploquin et al., 2004). The cave extends in an Upper Hettangian marbly limestone and dolostone formation, which constitutes one of the two unnamed formations distinguished within the Hettangian sediments of the Lozère department. This formation can be up to 100 m thick near Florac (Briand et al., 1979; Brouder et al., 1977; Gèze et al., 1980; Moreau et al., 2018).

3. Materials and methods

3.1. Sampling

All the samples in this study were collected from Malaval Cave (Lozère, France). To avoid destroying any speleothems, all samples were picked up on the ground. Samples consist of speleothems (stalactites, stalagmites) and fragments of the host rock. Blue and white speleothems were sampled at two different locations in the cave, to allow comparison within Malaval Cave’s setting. Depending on the amount of material available, the samples were then either crushed into powder and sieved at 125 μm or cut and prepared as thin or polished section (Table 1).

Among the sampled speleothems was a 30 cm-long blueish speleothem, identified as sample STAL (Fig. 3a). This structure is a stalactite, as shown by the presence of a central canal, and was previously broken by an unknown visitor, transported, and abandoned within the cave. Sample STAL was sawed in half to reveal strong color variations between successive crystallization layers, from white to green (Fig. 3b). Five distinct zones were determined within the speleothem based on growth discontinuities and color variation, from oldest to youngest: the white central canal (zone 1), a 0.5 cm-thick brown zone (zone 2), a 2.5 cm-thick whiteish zone (zone 3), a 2.5 cm-thick greenish zone (zone 4) and a 0.5 cm-thick white cortex (zone 5). The zones were measured at the stalactite base and their numbering refers to Fig. 3b. Each of these zones was subsampled to be crushed into powder and prepared as thin or polished sections.

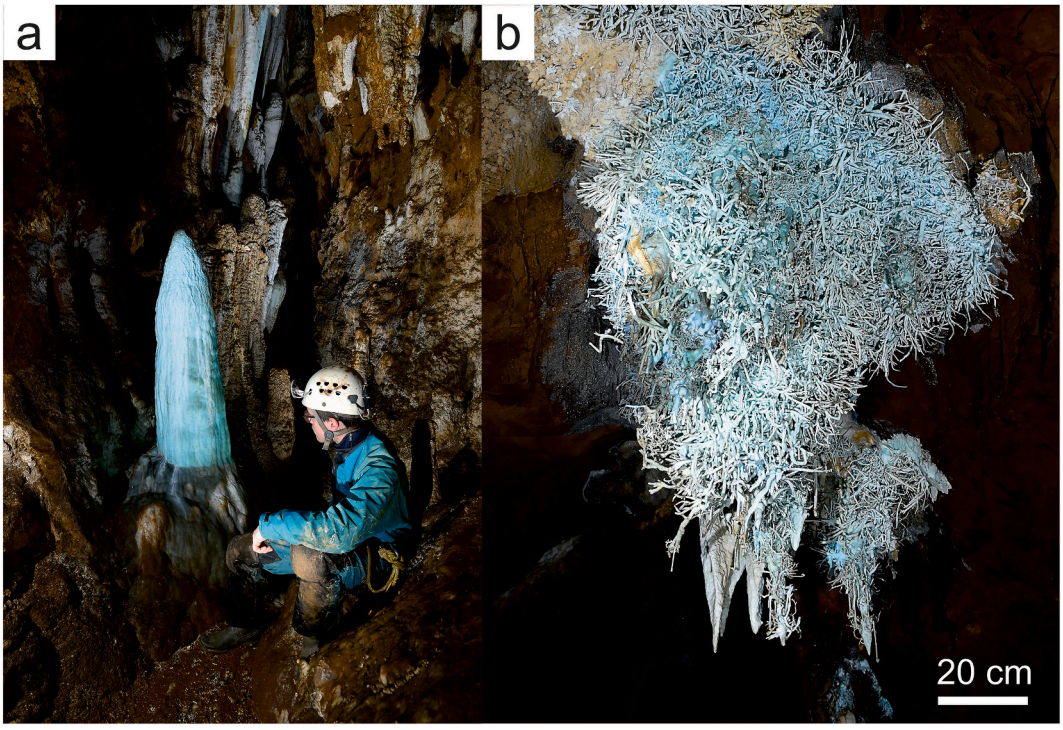

Fig. 1. a) Blue stalactite in Malaval Cave. b) Large blue coralloid aragonite structure overlying the main sampling site in Malaval Cave. (For interpretation of the references to color in this figure legend, the reader is referred to the web version of this article.)

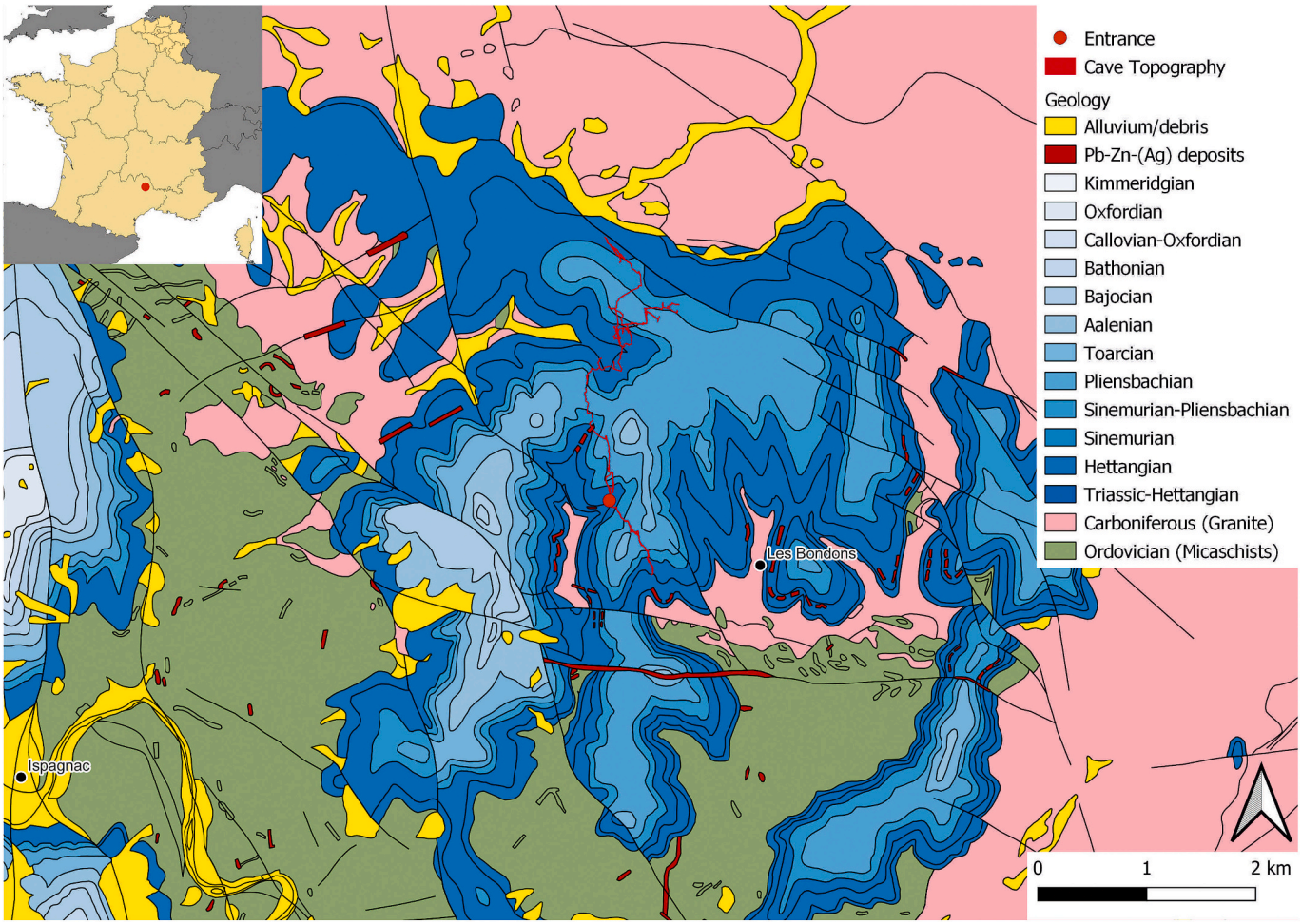

Fig. 2. Geological context of Malaval Cave. The Jurassic formations hosting the cave (Grands Causses) are subhorizontal and deposited on Ordovician micaschists and Carboniferous granite (Cevennes Massif) (Gèze et al., 1980).

Table 1
List of all samples used in this study, including their preparation methods.

Samples (simplified names)		Original names	Powder	Thin section	Polished section
Sample STAL parts (Fig. 3)	#1) Canal		X	X	X
	#2) Brown zone		X	X	X
	#3) White zone	22MALst	X	X	X
	#4) Greenish zone		X	X	X
	#5) Cortex		X	X	X
Blue samples	B1	22MAL01	X	X	X
	B2	22MAL02	X		X
	B3	22MAL06	X	X	X
	B4	22MAL08	X		X
	B5	22MAL09		X	X
	B6	22MAL10		X	X
White samples	W1	22MAL03	X	X	X
	W2	22MAL04	X		
Host rock	HR1	22MAL07	X		

3.2. Methods

Optical microscopy observations were made at the University of Namur on standard polished thin sections (thickness 30 μm, for transmitted light observations) and on samples mounted in epoxy resin and polished (for reflected light observations), using an Olympus Evident BX53M polarizing microscope coupled with an Olympus DP23 camera, and an Olympus BX61 microscope, combined with an Olympus XC50 camera and an Olympus BX-UCB light source. The former was used to acquire high-quality pictures, and the second to get spectrophotometry measurements coupled with pictures.

Polished sections were observed using a JEOL-7500F scanning electron microscope coupled with an Ultra Nine 30 JED-2300F Energy Dispersive X-ray Spectrometer (EDS). The samples were coated with ~20 nm of carbon (or gold when carbon quantification was required) using a Quorum Q150 T/ES to ensure good conductivity and avoid charge effects. Acceleration voltage was set to 20 kV. Observations were made using a backscattered electrons detector. Semi-quantitative EDS

Fig. 3. a) Colored stalactite sampled from Malaval Cave (sample STAL). The brownish color is due to some sediments and a hint of blue is visible in the lower part. b) Sawed slab. The zones are delimited and labeled with a number. 1 = central canal. 2 = brown growth zone. 3 = whitish growth zone. 4 = greenish growth zone. 5 = white cortex. (For interpretation of the references to color in this figure legend, the reader is referred to the web version of this article.)

analyses were obtained using the standardless method and ZAF correction.

The samples were grounded with a RETSCH PM 100 planetary ball mill, using opal bowls and marbles to avoid metal contamination. The powdered sample were then sieved using a 125 μm mesh. X-ray Diffraction (XRD) analysis was performed using an X-ray Panalytical X'Pert Pro diffractometer and a PHILLIPS PW3710 (CuKα radiation) at the PC^2 platform (UNamur), operating at 40 kV and 30 mA in the 5–70° 2θ range. CuKβ radiation was filtered out using a Ni filter placed along the diffracted beam path. One of the polished sections was directly analyzed with this technique, without being ground.

Mineral phases potentially undetected by XRD were analyzed by Raman microanalysis to determine their mineralogy using a Horiba Scientific LabRAM Soleil Raman confocal microscope. Raman spectra were recorded using an incident wavelength of 532 or 785 nm depending on the analyzed minerals. Laser power ranged from 1 mW to 20 mW, and acquisition time was set to 20 s. Both gratings (600 and 1800 lines/mm) were used, depending on the sample. Measurements were collected using the 50X objective and a confocal pinhole of 200 μm.

Powdered and sieved samples were geochemically analyzed at Activation Laboratories (Ancaster, Canada) by Inductively Coupled Plasma Mass Spectrometry (ICP-MS) and Inductively Coupled Plasma Optical Emission Spectrometry (ICP-OES) to obtain their bulk geochemical composition. Sample preparation was performed by lithium metaborate/tetraborate fusion and digestion of the molten beads in diluted nitric acid. Additional analyses (e.g., CO_3^{2-} content, organic matter) were performed by infrared spectroscopy.

ToF-SIMS measurements were performed using a ToF-SIMS IV instrument from IONTOF equipped with a 25 keV Bi^{1+} beam. A flood gun was used in combination with Ar flooding for charge compensation. Prior to the analysis, the sample was sputtered using an O_2 gun to clean the surface of contaminations (3 × 5 mm^2, 2 keV, 600 nA, 60 s, 1 × 1 mm^2 patches). Large area maps were performed in positive polarity in HC bunched mode, with the following settings: 4 × 2 mm^2 with patch size of 400 μm^2, 40 frames/patch and 200 pixels/mm. Data analysis was performed using Surface Lab 7.2 Software.

XPS measurements were performed using a K-alpha spectrometer from Thermofisher, equipped with a monochromatic Al Kα source (1486.6 eV). The Thermo Avantage software was used for data processing. Survey and high-resolution spectra were first performed on different regions of the surface (400-μm spot size) with an energy step of 1.0 and 0.1 eV, and a pass energy of 200 eV and 50 eV, respectively. Spectra recorded to perform the XPS map were measured using the so-called snapshot mode (with pass energy of 150 eV) using a 200-μm spot size. This mode allowed us to acquire faster images with sufficient count rates. A 2 × 5 mm^2 map was acquired with Ca2p, O1s, C1s, Sr3d, Ba3d and Pb4f measured in snapshot mode in each pixel in order to quantify the amount of Pb on the surface of the sample. Prior to the mapping, cleaning of the surface was performed using monoatomic Ar sputtering at 2 kV for 600 s (2 sputtering of 3.5 × 3.5 mm^2 were performed to cover the entire map area). A flood gun with combined electron and low energy ions was also used during analysis to prevent surface charging.

Optical microscope observations were performed using an Olympus BX61 microscope, combined with an Olympus XC50 camera and an Olympus BX-UCB light source. The reflection factor (reflected light intensity normalized to the intensity reflected by an Avantes WS-2 white diffusor and corrected for noise) was recorded with an Ocean Optics QE65 Pro spectrophotometer connected to the microscope. The measurements were performed at zero incidence and detection angles. Fluorescence microscope observations were performed with the same microscope and a Lumen Dynamics X-cite Series 120PCQ UV-lamp. The size of the analyzed spot on the elytron extended over several hundred square micrometers. From the reflection factor spectra, CIE 1931 xyY coordinates were calculated (Chamberlin and Chamberlin, 1980; Judd and Wyszecki, 1975) and converted into L*a*b* coordinates. L*a*b* coordinates are a set of three values calculated for each measured spectrum that allows an objective quantification of the color by placing it in a L*a*b* color space, where L* represents the saturation and a* and b* determine the hue (a* represents the green-red opponent colors and b* the blue-yellow opponent colors) (Chamberlin and Chamberlin, 1980).

In-situ trace element analyses on speleothem samples were performed by laser ablation inductively coupled plasma mass spectrometry (LA-ICP-MS) using a Teledyne G2 excimer laser coupled to a Thermo-finnigan Element XR ICP-MS (AETE-ISO regional facility of the OSU OREME, University of Montpellier). The instrument was tuned for maximum sensitivity and low oxide production (ThO/Th < 1 %). Analytical conditions are identical to those reported in previous studies (Bruguier et al., 2020) where ablation experiments were performed under helium, which enhances sensitivity and reduces inter-element fractionation (Günther and Heinrich, 1999). The helium stream and particles ablated from the sample were then mixed with pure nitrogen after the sample cell and subsequently with Ar before entering the plasma. Laser spot size was 50 μm for most analyses and down to 10 μm for silicate inclusions (e.g. nepouite) identified in the analyzed speleothems. Internal standard normalization was performed using CaO (56 wt % stoichiometric value for calcite and CaO + MgO = 56 wt% for dolomite), SiO_2 for silicate and ZnO for *Zn-bearing carbonates*. The laser was operated at a repetition rate of 6 Hz using a 4 J/cm^2 energy density. Total analysis time was 90 s with the first 45 s used for background measurement, which was subtracted from the sample signal. Before each analysis, the surface of the targeted zone was cleaned with 10 pulses, using a spot size larger than the size used for analysis. Trace elements were calibrated against the reference glass material NIST 612 (values after (Pearce et al., 1997)). Accuracy of the analyses was monitored using the carbonate reference material MACS-3 (values taken from GEOREM preferred values) and was always better than 15 %. Raw data were reduced using Glitter software (Van Achterberg et al., 2001).

4. Results

4.1. Color characterization

Optical spectrophotometry results show that the blue color observed

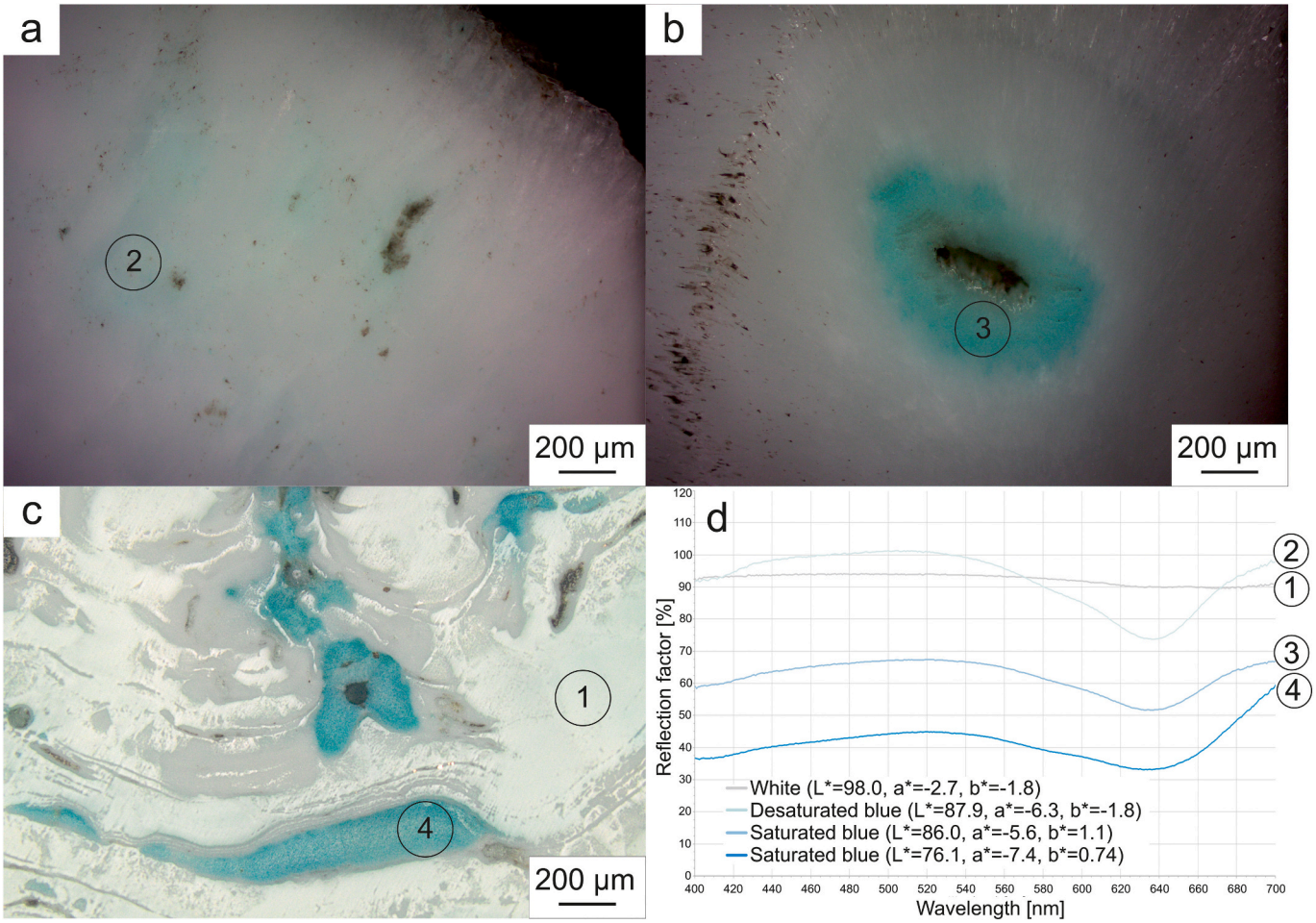

Fig. 4. Variations of the blue color within the samples. a) Sample B4. b) Sample B2. c) Sample W1. d) Reflection factor spectra measured on 4 variously colored zones. Calculated L*a*b* coordinates are indicated between brackets. (For interpretation of the references to color in this figure legend, the reader is referred to the web version of this article.)

within the speleothems is not homogeneous, which can be observed with the naked eye in most samples. Fig. 4a-d displays the reflection factor spectra of differently colored zones, referred to as "white", "desaturated blue" and "saturated blue" in this document. White zones are characterized by a nearly flat spectrum approaching 100 % reflection factor. Desaturated blue zones show a similarly high reflection factor but also a variation of about 25 % between the most reflective wavelength (about 510 nm) and the least reflective one (about 635 nm). Saturated blue zones are characterized by a similar profile (highest reflection at 510 nm and lowest at 635 nm), but with a much lower reflection factor. The most saturated blue color is observed in sample W1 (Fig. 4c, d), which is also the only macroscopically white sample containing blue phases. Mean calculated L*a*b* coordinates for each zone are included in Fig. 4d.

4.2. Mineralogical composition

XRD measurements show that the host rock from the cave is composed of calcite and is sometimes intersected with quartz veins, which is consistent with the data in the geological map (Gèze et al., 1980). Each speleothem sample from Malaval cave is almost exclusively composed of aragonite, as no other mineral phase is detected, neither in the blue ones nor in the white ones. Zones 1 and 3–5 of sample STAL (Fig. 3b) are composed of aragonite and zone 2 is composed of calcite. Sample W1 contains blue phases in its central part (Fig. 4c). XRD analyses performed directly on this polished section, focused on the blue zone, do not allow a determination of the unknown mineral.

Raman micro-spectroscopy was used on the blue phases of sample W1 (Fig. 4c) to determine their mineralogical nature. All measurements show a total absence of Raman features. A significant luminescence is observed in every spectrum, making the identification impossible. Raman measurements were also performed on sample B2 using a 532 nm laser, to assess the potential presence of a (mineral) phase in the saturated blue area (Supp. data fig. 1). The Raman fingerprint is very similar between saturated and desaturated zones and corresponds to aragonite only. The measurements performed on the saturated zone exhibit a much higher luminescence than on the desaturated zone. This could be explained by the presence or absence of blue coloration. Measurements performed on the same saturated blue zone using the 785 nm laser also do not show any Raman feature other than aragonite, though with much less luminescence. This suggests that the saturated blue zone does not contain any mineral phase other than aragonite, which is consistent with the microscopical observations.

Electron microscope observations performed on the macroscopically blue sample (listed in Table 1) show the presence of higher Z spots of about 2–3 µm in diameter in some of them (Fig. 5a). EDS analyses performed on these spots and on the surrounding aragonite matrix show that i) no metallic elements other than Ca are detected in the aragonite matrix, and ii) the high Z spots all contain Cu, O, Zn, Si and Ca in highly variable concentrations (Supp. data table 1). By comparing Zn and Ca concentrations at each analyzed point, a strong inverse correlation is observed (R^2 = 0.91), with points exhibiting the highest Zn

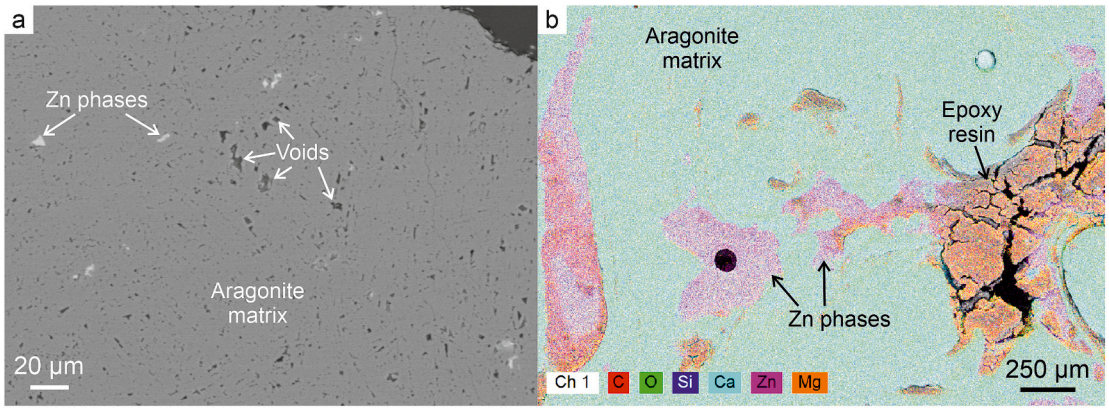

Fig. 5. a) SEM backscattered electrons view of the blue aragonite sample B4 showing several high-Z spots (white). See Supp. data table 1 for EDS results on these spots. b) EDS mapping on the amorphous Zn-bearing phases in sample W1 (Fig. 4c). See Supp. data table 2 for EDS results on these phases. (For interpretation of the references to color in this figure legend, the reader is referred to the web version of this article.)

concentration showing almost no Ca. This suggests that the high Z spots most probably do not contain any Ca and that the detected Ca is part of the surrounding matrix, due to the very small size of the grains. Although the EDS analyses do not allow a fully quantitative analysis, it can be concluded that the higher Z spots are composed of a phase highly enriched in Zn and contain variable amounts of Cu, Si, O and C. The latter was not dosed because the samples were coated with carbon, but the high carbon signal likely indicate the presence of carbon in the Zn phases.

EDS analyses were performed on the larger phases of sample W1, which also contain high amounts of Zn (Fig. 5b). Although similar, these yielded slightly different results compared to the micrometric phases in other samples, including the detection of several wt% Mg (Supp. data table 2). Cu was not detected, showing it is likely <1000 ppm. The sample was coated with Au rather than C to allow carbon quantification. These results show that the blue phases contain major amounts of Zn, O and C, as well as significant amounts of Si and Mg, but no Ca. The measured compositions are close to the smaller Zn-rich spots presented before.

Sample B3 is the only one where a significant amount of Pb is detected by the EDS. The Pb was found in concentric rings along the outer part of the speleothem, which appear darker than the surrounding Pb-depleted aragonite in optical microscopy (Fig. 6a). The dark rings yielded 0.33 to 1.49 wt% Pb (respectively points B3_5 and B3_2 in Fig. 6b) and were progressively more enriched towards the outer border. No Pb is detected between the rings.

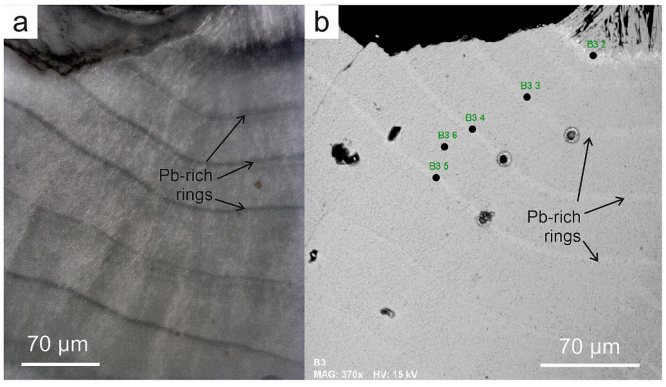

Fig. 6. a) Optical microscope and b) SEM backscattered electrons view of sample B3. The dark rings in (a) appear white in (b) due to their higher Pb content. The black dots labeled in green represent points analyzed by EDS. (For interpretation of the references to color in this figure legend, the reader is referred to the web version of this article.)

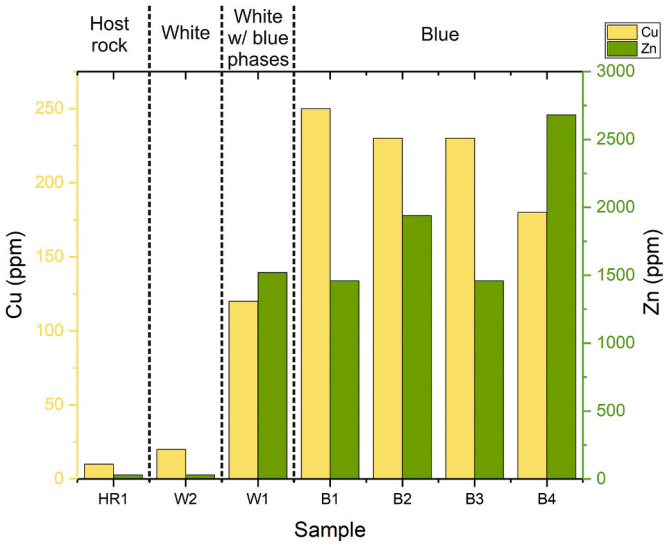

Fig. 7. Cu and Zn concentrations in the host rock and speleothem samples, separated by observed macroscopical color. Sample W1 (Fig. 4c) is separated from the other samples as it appears white macroscopically despite containing blue phases observed by optical microscopy. (For interpretation of the references to color in this figure legend, the reader is referred to the web version of this article.)

4.3. Geochemical composition

Bulk chemical analyses (ICP-MS) on the blue samples (Supp. data table 3) stress the presence of unusually high concentrations of Cu (up to 250 ppm), Zn (up to 2680 ppm), Sr (up to 2504 ppm), Pb (up to 426 ppm) and Ba (up to 329 ppm). In Fig. 7, Cu and Zn concentrations are compared with the macroscopical color of the samples (white or blue). First, every blue sample has a bulk Cu concentration of at least 180 ppm, typically exceeding 200 ppm, while the white samples show lower Cu concentrations ranging from 20 to 120 ppm. The Zn concentration is consistently much higher than the Cu concentration, yielding at least 1460 ppm in blue samples. 1520 ppm of Zn was detected in macroscopically white sample W1, likely due to the Zn-rich blue phases observed by SEM (Fig. 4c). Sample W2 is largely depleted in Zn and Cu, with concentrations of <30 ppm and 20 ppm, respectively. The Sr concentration in speleothems is at least 1039 ppm, regardless of the sample color, and 140 ppm in the host rock. The Pb concentration is noticeably high in two blue samples (185 and 426 ppm) and ranges from 30 to 70 ppm in other speleothem samples, regardless of their color,

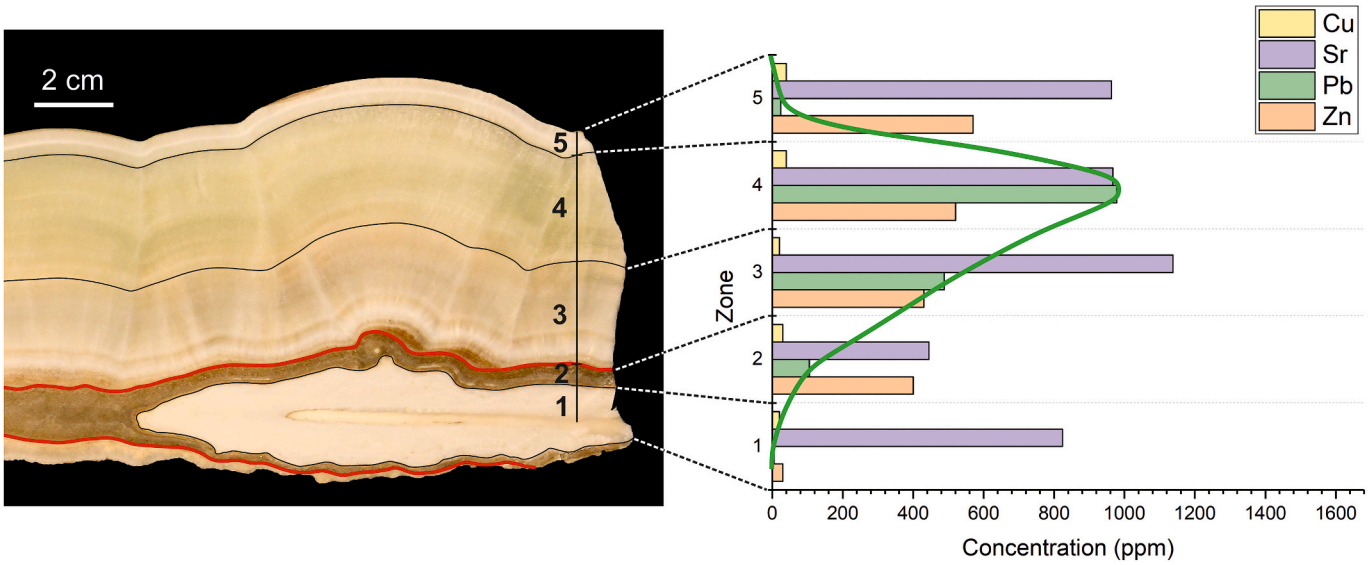

Fig. 8. Bulk ICP-MS results of each major zonation in sample STAL. The graph on the right shows the Cu, Sr, Pb and Zn concentrations for each zonation. Pb concentration variation is highlighted by a green line. (For interpretation of the references to color in this figure legend, the reader is referred to the web version of this article.)

except for sample W2 which is devoid of Pb. The R^2 values comparing the metal concentrations (Supp. data table 4) clearly show that most of the metals do not correlate strongly with one another across the various samples, except for Cu and Zn which have a notably higher R^2 value of 0.61.

The analyses performed on sample STAL show major compositional differences, both when compared to the smaller blue stalactites and within the sample itself. In this sample, the Cu concentration ranges from 10 to 40 ppm, which is much lower than in the blue stalactites, while significant amounts of Zn, Pb and Sr are detected (Fig. 8). These measurements highlight strong variations between each major zonation of the speleothem, where the concentrations of the various metals are poorly correlated (Supp. data table 5). Nevertheless, the Pb concentration appears to be closely associated with the green color, being especially concentrated in the green zone (zone 4) and much lower in the other zones.

ToF-SIMS analyses were performed on the transition between zones 3 and 4 of sample STAL (Fig. 3b) to estimate the potential correlation between the measured intensity of the green color and the relative concentrations of various metallic elements. As the mappings performed before oxygen blasting showed traces of contamination, only the ones performed after blasting were studied. ToF-SIMS results confirm the ICP-MS results, though with a spatial resolution of a few micrometers. The only element with a significantly different concentration between the green (4) and white (3) zones is Pb, which shows a peak at the limit between both zones and rapidly decreases in the white zone (Fig. 9). All other elements either show a very low concentration (e.g., Cu, Zn) or do not show any significant variation (Ba, Sr).

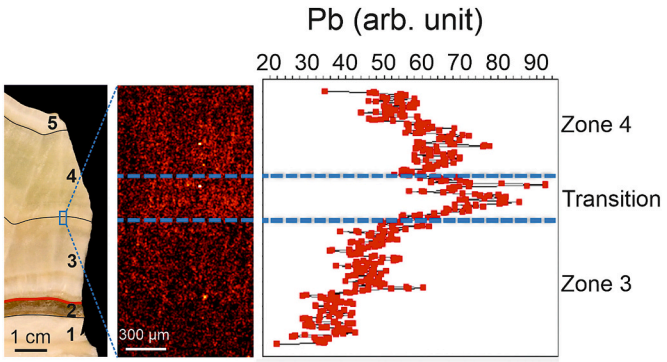

Fig. 9. ToF-SIMS mapping of the Pb signal on the limit between the zones 3 and 4 of sample STAL (blue rectangle on left-hand picture, to scale). The horizontal blue lines delimit the transition between both zones, characterized by a thick yellowish line in the sample. (For interpretation of the references to color in this figure legend, the reader is referred to the web version of this article.)

XPS results on sample STAL refine the ToF-SIMS results by allowing quantification (Supp. data fig. 2). This is particularly useful in the transition between the greenish and whitish zones (resp. zones 4 and 3 of sample STAL). A clear decrease in the Pb concentration is observed towards the whitish zone (from 1500-2000 to 720 ppm), with a higher concentration observed at the limit between the zones (about 3700 ppm). These values are in agreement with the ToF-SIMS results described above (Fig. 9) and confirm the chemical variations between the differently colored zones in this sample.

LA-ICP-MS measurements were performed on blue and white speleothem samples, as well as on all the different sections of sample STAL, for a total of 278 points on 14 samples (either on polished or thin sections). The measurements were conducted to facilitate the comparison of the variously colored zones within each sample and between samples, aiming to assess the potential causes of the coloration.

First, a general comparison of all the points analyzed showed some trends that are observed in each sample. The minor elements, often yielding at least 1000 ppm, are always Si, Zn, Sr, Pb and Ba, which are also observed in the bulk ICP-MS results. These elements' concentrations vary significantly between samples and within samples. Considering the trace elements (i.e. <1000 ppm), Cu is generally the most concentrated (about 150–250 ppm in blue samples), while Fe, Ni and Mn are generally associated with Pb. Finally, Mg occurs mostly in the presence of Zn, and Cu also shows a good correlation with Zn (mostly when Pb is absent). The Zn/Cu ratio for every point analyzed is comprised between 7.5 and 30. As inferred by the bulk ICP-MS results, the mean Cu content is clearly different between blue aragonite (153–260 ppm) and white aragonite (13–35 ppm). The distinction is less clear for the Zn concentration, yielding 1232–4501 ppm in blue aragonite and 10–5288 ppm in white aragonite.

Strong variations are observed between the blue-colored zones within some samples, most clearly in sample B2 (Fig. 10a-c). In this sample, a localized saturated blue zone is present on the periphery of a hole (Fig. 10b). Analyses within this zone reveal a sharp increase in Pb

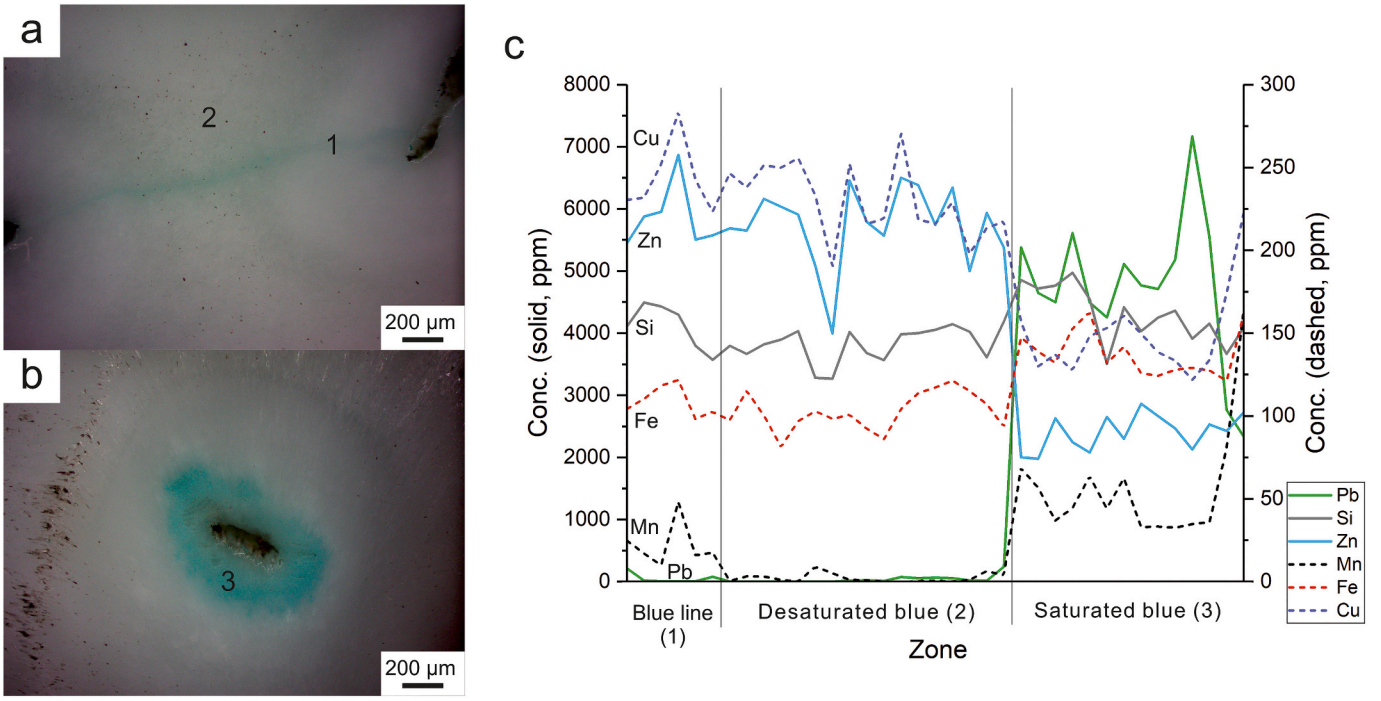

Fig. 10. a) and b) Optical microscope views of sample B2, highlighting the variously colored zones analyzed by LA-ICP-MS. 1 = blue line, 2 = desaturated blue, 3 = saturated blue. c) LA-ICP-MS results separated based on the color of the analyzed zone. The scale of the dashed lines is on the right-hand side of the graphs. Numbers correspond to the zones shown in a and b. (For interpretation of the references to color in this figure legend, the reader is referred to the web version of this article.)

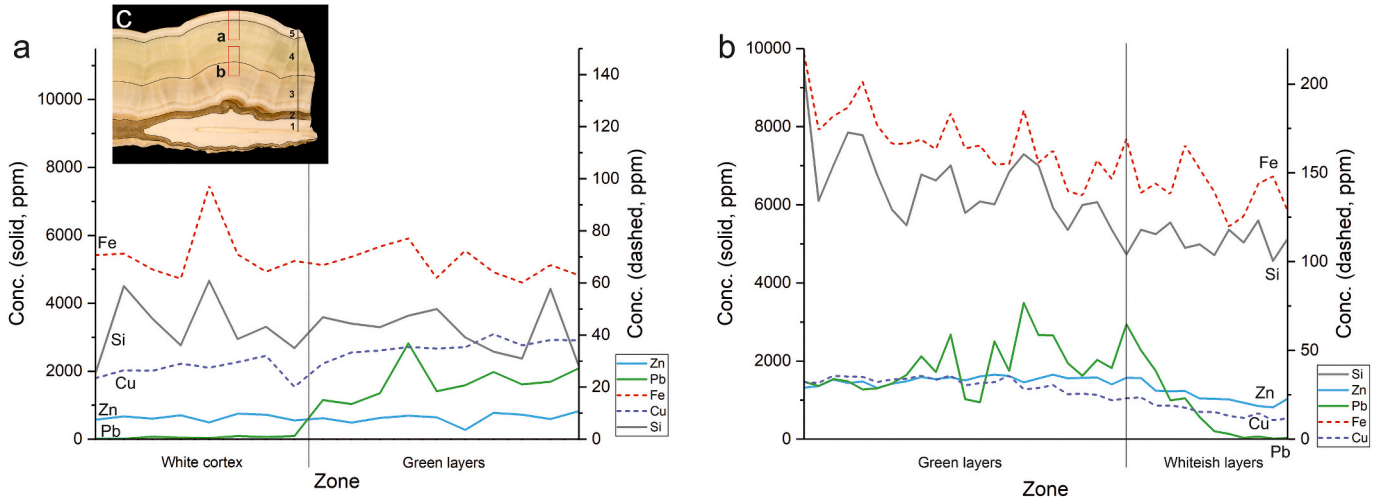

Fig. 11. LA-ICP-MS measurements performed on sample STAL. The scale of the dashed lines is on the right side of the graphs. a) Zones 5 and 4 (outermost part of the stalactite). b) Transition between zones 4 and 3 (green to white). c) Visualization of the analyzed zones on the whole sample. (For interpretation of the references to color in this figure legend, the reader is referred to the web version of this article.)

concentration along with a lesser increase in Mn and Fe concentrations. A sharp decrease in Zn and Cu concentrations is observed in this same zone.

The trace concentrations measured in sample STAL are generally lower than in sample B2, which concurs with the less saturated coloration observed within this sample. As mentioned in Section 3.1, this stalactite was divided into 5 zones, from oldest to youngest: a white aragonite central canal; a brownish calcite zone; a whitish aragonite zone; a greenish aragonite zone and a white cortex (Fig. 3b). LA-ICP-MS analyses refine the ICP-MS measurements and show some geochemical trends (Fig. 11a-c).

There are significant differences between the white cortex and the greenish zone, mostly considering Pb. While the cortex is completely devoid of Pb, the greenish zone contains about 2000 ppm and up to 3500 ppm of Pb. The Cu concentration is low in both zones (about 30–40 ppm) and increases slightly towards the greenish zone. Zn and Fe are quite constant through both zones. Going inward to the transition between zone 4 (greenish) and zone 3 (whitish) of the stalactite, the concentration of each element analyzed steadily decreases. Among all these elements, Pb shows the steepest decrease, and is the only one approaching 0 ppm towards the center of the whitish zone. As shown with the first ICP-MS results (Fig. 8), several trace elements exhibit strong concentration variations between the different zones, but Pb displays the best association with the occurrence of the green coloration

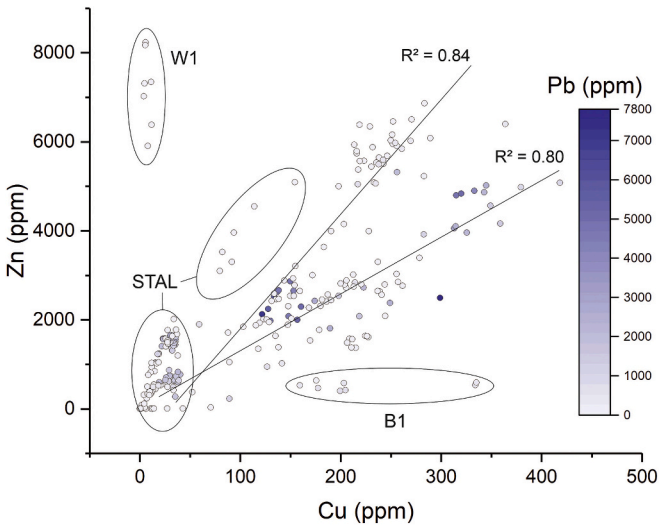

Fig. 12. Linear regression between Zn and Cu concentration in every point analyzed by LA-ICP-MS. The symbols are colored according to the Pb concentration. R^2 for both trends do not include the circled points (samples B1, W1 and STAL).

within sample STAL.

Across all samples, every analyzed point with a Pb/Zn ratio >1 exhibits a blue or greenish coloration of varying intensity, or at least a darker hue compared to the zones with less Pb concentration, confirming the EDS measurements (Fig. 6).

The LA-ICP-MS analyses on the Zn-rich blue phases from sample W1 (Fig. 4c) confirm that these phases are largely Ca and Pb-depleted, as shown by the EDS analyses (Supp. data table 2), suggesting that they are not composed of aragonite and ruling out Pb as the coloration cause in this sample. A significant Cu concentration is also detected in these phases.

Thanks to the large number of LA-ICP-MS analyses performed on every sample, it is possible to check the correlation between Cu and Zn in much more detail, at microscopic level. Fig. 12 displays this correlation and allows comparison with their Pb concentration as well. If we exclude points from sample W1, that are largely Cu-depleted, and points from sample B1, that are Zn-depleted, two main trends arise (a Zn-enriched one, $R^2 = 0.84$, and a Zn-depleted one, $R^2 = 0.80$). The Pb gradient shows that every point containing a significant amount of Pb (i.e. represented by saturated blue dots in Fig. 12) is located on the Zn-depleted trend.

4.4. Structural variations

Several close-up shots of the white and blue parts in sample B2 were taken in secondary electrons view (Supp. data fig. 3) to analyze the fine structure of the speleothems and assess the presence or absence of photonic structures, which could induce light-wave interference. Photonic crystals are characterized by periodic structures (generally layers) of a size close to visible light wavelength. Photonic structures have dimensions in the order of visible light wavelength (i.e. about half a micron) and scatter incident light (Joannopoulos, 2008; Mouchet and Deparis, 2021).

These views do not reveal clear photonic structures active in the visible part of the electromagnetic spectrum giving rise to structural color but still show an obvious difference in porosity and crystalline structure between the blue and white zones of this sample. As this difference in textures coincides with the presence or absence of elevated Pb concentrations, it can be inferred that the presence of high amounts of Pb^{2+} in substitution within the aragonite can induce textural changes.

5. Discussion

In this article, we aim at unravelling the causes of the blue to green coloration of aragonite speleothems in Malaval Cave. Significant concentrations of various metals, including Pb, Cu, Zn and Sr, are detected within the speleothem samples, and some of them, especially Cu, are often reported to induce a blue coloration (Cairncross, 2004; Turner, 2002). Metals can therefore be considered as relevant causes for the observed coloration. However, several issues must be answered, including i) which element(s) play a role in the coloration and which do not, ii) whether the coloring element(s) are present in substitution in the aragonite or as separated (mineral or amorphous) phases, and iii) what the origin of the metallic elements is.

5.1. Cu^{2+} as the main cause of the speleothem coloration

Considering all the results presented in this work, we propose Cu^{2+} substituting for Ca in the aragonite as the primary cause of the desaturated blue coloration both microscopically and macroscopically.

Zn and Cu concentrations are quite well correlated both in bulk and spatially resolved analyses, and Zn/Cu ratios are consistently high in each blue sample. According to the literature however, Zn^{2+} in substitution within aragonite or calcite could not be responsible for any coloration, due to the electronic distribution of the Zn^{2+} ion (White, 1997). Thus, Cu concentration is a much more likely cause. First, Cu^{2+} substitution is commonly associated with a blue to green coloration in a variety of minerals, including aragonite. Additionally, Cu^{2+} creates a similar blue-green coloration when substituting for Zn within smithsonite (Ding et al., 2023; Samouhos et al., 2015). Cu is significantly present in every analyzed point on macroscopically blue aragonite, but not in any white or greenish sample, which is clearly observed both in the bulk and spatially resolved analyses. This is not observed for Zn, as shown in Section 4.3. All these arguments support the hypothesis that Cu^{2+} ions are responsible for the desaturated blue coloration in the aragonite and allow us to further propose that Zn^{2+} likely do not have any impact on the blue coloration.

5.2. Impact of blue Zn-bearing phases on the speleothem coloration

Although Zn^{2+} substitution was ruled out as a coloration cause, the matter of the amorphous Zn-bearing carbonate phases disseminated in the matrix of some samples remains to be addressed. These phases exhibit a saturated blue color, thus likely impacting the speleothems' coloration.

The amorphous state of the Zn-rich phases can be associated with early supergene mineral structures linked to metal ores (sometimes called "gels") (Lambiel et al., 2023; Perruchot et al., 2001). These structures are amorphous and poorly organized, making their determination difficult by classical mineralogical methods. The precipitation of amorphous gels constitutes generally the primary phase created by weathering (Perruchot et al., 2001). Zn-bearing gels are common precursors of other supergene mineral phases such as hemimorphite, smithsonite or hydrozincite. If the gel phases are dried before their recrystallisation, they may stay in their amorphous state (O'Day et al., 1998). Gels are commonly associated with metal-rich groundwaters at the vicinity of metallic ores and their composition can be very diverse. The nature of the precipitated gels usually depends on the metal concentrations in the water and on the pH conditions (Dutrizac and Chen, 1987; Lambiel et al., 2023). Zn-bearing phases are commonly formed in basic conditions, often found in carbonaceous rocks at a pH ~ 8 (Steinberg et al., 1985) which corresponds to a karstic cave setting.

The Zn-bearing gels in Malaval Cave are disseminated in the aragonite matrix of some blue speleothems as 2–5 μm inclusions (Fig. 5a). As these phases exhibit a saturated blue color, we propose that they likely influence the coloration of the speleothems in which they are present. This might explain the high variability of the blue coloration hue and

saturation throughout the samples, as these variations cannot be explained solely by the Cu^{2+} concentration. Though Cu^{2+} ions substitution remains the primary coloration cause in all blue samples analyzed as explained in Section 5.1, Zn-bearing gels likely play a significant role in the observed color variations.

5.3. Pb^{2+} substitution as a cause of the speleothem coloration

No Pb-bearing phase has been identified in any sample from Malaval cave, suggesting that Pb is solely present as Pb^{2+} substituting for Ca^{2+} in the aragonite. It is possible for aragonite and calcite to incorporate some Pb while staying homogeneous before converting to cerussite (Di Lorenzo et al., 2019). This type of substitution is commonly found in the weathering zone of Pb deposits (Bouabdellah et al., 2021; Poot et al., 2024; Takahashi, 1960; Verhaert et al., 2017) which corresponds to the cave's setting (Gèze et al., 1980; Ploquin et al., 2004).

Our results show a probable link between the presence of Pb and the green coloration in sample STAL and B3, as well as with the saturated blue coloration in samples B2 and B1. Thanks to their good spatial resolution, the LA-ICP-MS results (Fig. 10a-c, Fig. 11a, b) clearly highlight the association between the Pb concentration and the green or saturated blue color. Still, the saturation and hue of the color cannot be linked to the absolute Pb concentration, and some Pb-rich zones are devoid of color. Moreover, saturated blue zones in sample B1 contain less Pb than greenish zones in sample STAL. Thus, while a link between the presence of Pb^{2+} in substitution and a green to blue coloration is clear in several samples, it is difficult to propose a definitive explanation regarding these color variations. Considering all the results, our preferred hypothesis is that the presence of Zn^{2+} ions might inhibit the coloration induced by the Pb^{2+} ions. This hypothesis is explored in Section 5.4.

5.4. Zn-Cu-Pb interactions

Considering the geochemical similarity of Cu, Zn and Pb and the fact that all three elements probably share the same origin (see Section 5.6), interactions between those metals potentially impacting the coloration must be discussed. Of all three, Cu seems to show less interaction, as Cu^{2+} ions create a desaturated blue coloration relative to their absolute concentration, independently of Pb and Zn concentrations. The fact that Cu is mostly found in the presence of Zn merely suggests that both were comprised in the same mineralizing fluids at some point of the speleothems' deposition. This covariation does not significantly influence coloration.

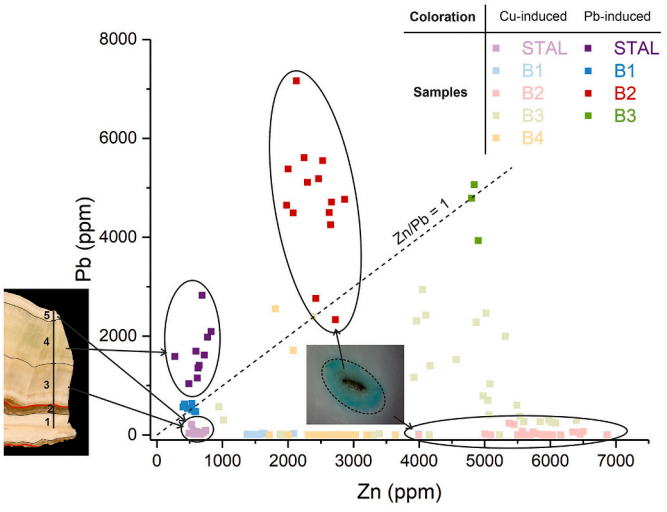

Fig. 13. LA-ICP-MS results for every colored sample focused on Pb and Zn concentrations. Points are classified depending on the sample and on the proposed cause of the coloration. The diagonal line represents a Pb/Zn ratio of 1. Microscopic views of samples STAL and B2 are included to illustrate color variation.

Pb—Zn interaction seems to have a direct influence on the observed coloration. This is suggested by the link between Pb-induced coloration and elevation of the Pb/Zn ratio, as proposed in Section 5.3. LA-ICP-MS results show that Pb-rich zones are generally Zn-depleted, indicating that Zn and Pb are at least partially mutually exclusive. This can be explained by the difference in fluid affinity between Zn and Pb, and by dissolved content variations in the mineralizing fluids (Skarpelis and Argyraki, 2009). The only zones with high Pb concentrations that do not exhibit significant coloration always contain high Zn concentrations. These observations suggest that the presence of Zn^{2+} alongside Pb^{2+} could have a significant impact on Pb-induced coloration, as shown in Fig. 13.

This figure shows that Pb-induced coloration is only present in zones where the Pb/Zn ratio is roughly higher than 1, regardless of the absolute Pb and Zn concentrations. It suggests that, when substituting for Ca in the aragonite and in the context of Malaval Cave, Pb^{2+} ions induce a green to blue coloration whenever they are at least equally concentrated than Zn^{2+} ions. As mentioned in Section 5.1, high amounts of Zn^{2+} in substitution do not induce any coloration, unlike Zn-bearing gels. Considering this, we propose that Zn^{2+} ions may inhibit the coloring action of Pb^{2+} ions. This proposed inhibitory effect was never reported in literature. Still, it can be compared to other occurrences where metallic ions exhibit decolorizing effects on textile dyes (Zafiu et al., 2021). Although the exact nature of the interaction between Pb^{2+} and Zn^{2+} ions cannot be unequivocally determined with the results presented here, this hypothesis is supported by observations made in another cave, as explained in Section 5.5.

5.5. Comparison with blue speleothems from another cave (Crovassa Azzurra, Sardinia)

The results discussed in this work can be compared to the observations made on a blue and green-colored flowstone from Crovassa Azzurra (Sardinia) (Caddeo et al., 2011), which is the only documented occurrence we found of a Pb- and Zn/Cu-related blue-green coloration in a cave. The colors and chemical compositions observed in this cave are close to those found in Malaval Cave. In Crovassa Azzurra, chemical results also show that: i) there is a significant covariance between Zn and Cu concentrations, and ii) the aragonite zones containing the most Zn and Cu exhibit a desaturated blue color. Moreover, the two blue aragonite zones from Crovassa Azzurra cave are separated by a more greenish zone, much like zone 4 in sample STAL (Fig. 3b). This zone is much more Pb-rich than the others and is also the only zone with a Pb/Zn ratio higher than 1. This Pb is present as Pb^{2+} in substitution within the aragonite and in micrometer-sized cerussite crystals, the latter of which are absent in Malaval Cave. However, the zone containing more cerussite is also less green, further indicating that the green coloration is associated with a Pb^{2+} substitution in the aragonite. Although their work does not focus on the origin of the coloration in Crovassa Azzurra, the findings in Caddeo et al. (2011) clearly support the conclusions proposed here.

5.6. Origin of the metallic elements

Although the carbonaceous Jurassic formations hosting Malaval Cave are much younger than the main magmatic events that created the Cevennes Massif during the Carboniferous, the subsequent uplift and horsting event reactivated the magmatic activity, leading to extensive hydrothermal Pb-Zn-Ag hypogene ores (Fig. 2) (Bouladon, 1960; Brouder et al., 1977). These ores were mined from Antiquity to the Middle Ages (Ploquin et al., 2003; Prassl, 1997). Furthermore, these deposits are mostly found in the Upper Hettangian dolomitic formations, which are located just above the host formation of Malaval Cave (Gèze et al., 1980). Among the geographic sectors known to host Pb—Zn

mineralization, the sector of Montmirat-Les Bondons, where the cave is situated, was heavily exploited (Ploquin et al., 2004). Furthermore, amorphous gel-like Zn phases, which were found in our samples, are commonly found in the supergene zone of Zn deposits (Hitzman et al., 2003; Mondillo et al., 2011). Considering all this, we propose that Zn, Pb and Cu are directly linked to the nearby metallic ores.

The Pb/Zn/Cu ratios and covariation (Fig. 12, Fig. 13) further suggest that Zn and Cu were mostly deposited from the same mineralizing fluids, but Pb was deposited from different ones. The spatial variations in metal concentrations are a clear indicator that the metal content in drip water fluctuated strongly over time. No drip water samples were collected in Malaval Cave. Still, the relative abundances suggest that the mineralizing fluids contained mostly Zn, with minor amounts of Pb and Cu.

6. Conclusion and perspectives

The blue color of speleothems is commonly associated with the substitution of Cu^{2+} in the aragonite matrix. Here we suggest that Pb, Zn and Cu can contribute to the coloration to varying degrees. Firstly, our results suggest that Cu^{2+} substitution is the main cause for the macroscopical blue coloration. Secondly, microscopical colorations are affected by the presence of a high amount of very small Zn-bearing phases (probably "gels", with a chemical composition close to a Zn-bearing carbonate with significant Cu and Mg traces), dispersed within the aragonite matrix. Thirdly, the presence of a scarcer Pb^{2+} substitution creates a greenish or saturated blue coloration. Results suggest some level of metallic interaction between Pb and Zn, through which the Pb^{2+} coloring action may be inhibited by Zn^{2+} substitution, explaining the observed variations. The various chalcophile elements detected in Malaval cave likely originate from the Zn—Pb deposits localized in the vicinity of the cave and were transported to the cave by successive mineralizing fluids with various Zn, Pb and Cu content. Further investigations on this matter could include i) more refined analyses to unravel the precise link between Cu, Zn and Pb precipitation within the speleothems from Malaval Cave, ii) stable isotope analysis of the chalcophile elements to confirm their presumed origin, iii) dating of the samples to constrain the timing of deposition and coloration, and iv) drip water collection and analysis to assess the spatial variations between mineralizing fluids.

Declaration of conformity

We hereby declare that every sample from this study was picked up with the authorization of Jean-Louis Galéra, one of the cave's administrators.

CRediT authorship contribution statement

Martin Vlieghe: Writing – original draft, Visualization, Methodology, Investigation, Formal analysis. **Gaëtan Rochez:** Writing – review & editing, Resources, Investigation, Conceptualization. **Stéphane Pire-Stevenne:** Writing – review & editing, Resources. **Alexandre Felten:** Writing – review & editing, Resources, Formal analysis. **Marie Dechamps:** Writing – review & editing, Resources, Formal analysis. **Sébastien R. Mouchet:** Writing – review & editing, Resources, Formal analysis. **Francesca Cecchet:** Writing – review & editing, Resources. **Olivier Bruguier:** Writing – review & editing, Resources, Formal analysis. **Jean-Louis Galéra:** Writing – review & editing, Resources, Project administration. **Gipsi Lima-Mendez:** Writing – review & editing, Supervision, Conceptualization. **Marc Llirós Dupré:** Writing – review & editing, Supervision, Conceptualization. **Johan Yans:** Writing – review & editing, Supervision, Resources, Project administration, Conceptualization.

Declaration of competing interest

The authors declare that they have no known competing financial interests or personal relationships that could have appeared to influence the work reported in this paper.

Acknowledgements

M.V. acknowledges a UNamur FSR grant (1 year) followed by a Research Fellow grant from the Belgian National Fund for Scientific Research (F.R.S.-FNRS, convention FC 050205). S.R.M. was supported by a BEWARE Fellowship (Convention n°2110034) of the Walloon Region (CO-FUND Marie Skłodowska-Curie Actions of the European Union #847587), as a Postdoctoral Researcher. F.C. was supported by FRS-FNRS as a Research Associate. This research used the equipment from the Morphology & Imaging Platform (https://www.poledenamur.be/en/platforms/morph-im/equipment/electron-microscopy): Electron Microscopy; the Physico-Chemical Characterization (PC^2) Technology Platform (https://platforms.unamur.be/pc2): X-ray Diffraction; the Laser, Optics and Spectroscopies (LOS) Technology Platform (https://platforms.unamur.be/los): Optical Spectrophotometry, Raman Micro-spectrometry; and the Synthesis, Irradiation and Analysis of Materials (SIAM) Technology Platform (https://platforms.unamur.be/siam): Time-of-Flight Secondary Ion Mass Spectrometry, X-ray Photoelectron Spectroscopy. LA-ICP-MS measurements were performed at Géosciences Montpellier.

Appendix A. Supplementary data

Supplementary data to this article can be found online at https://doi.org/10.1016/j.chemer.2025.126285.

References

Baron, S., Carignan, J., Laurent, S., Ploquin, A., 2006. Medieval lead making on Mont-Lozère Massif (Cévennes-France): tracing ore sources using Pb isotopes. Appl. Geochem. 21, 241–252. https://doi.org/10.1016/j.apgeochem.2005.09.005.

Blyth, A.J., Smith, C.I., Drysdale, R.N., 2013. A new perspective on the $\delta^{13}C$ signal preserved in speleothems using LC-IRMS analysis of bulk organic matter and compound specific stable isotope analysis. Quat. Sci. Rev. 75, 143–149. https://doi.org/10.1016/j.quascirev.2013.06.017.

Bouabdellah, M., Boukirou, W., Potra, A., Melchiorre, E., Bouzahzah, H., Yans, J., Zaid, K., Idbaroud, M., Poot, J., Dekoninck, A., Levresse, G., 2021. Origin of the Moroccan Touissit-Bou Beker and Jbel Bou Dahar supergene non-sulfide biomineralization and its relevance to microbiological activity, late Miocene uplift and climate changes. Minerals 11. https://doi.org/10.3390/min11040401.

Bouladon, J., 1960. Sur les mineralisations en plomb-zinc et en antimoine de la peripherie du Mont-Lozere. Bull. la Société Géologique Fr. S7-II, 906–914.

Briand, B.-G., Couturié, J.-P., Geffroy, J., Gèze, B., 1979. Notice explicative de la feuille Mende à 1/50000. Bur. Rech. Géologiques Minières, Orléans, p. 52.

Brouder, P., Gèze, B., Macquar, J.-C., Paloc, H., 1977. Notice explicative de la feuille Meyrueis à 1/50000. Bur. Rech. Géologiques Minières, Orléans, p. 29.

Bruguier, O., Caby, R., Bosch, D., Ouzegane, K., Deloule, E., Dhuime, B., Bendaoud, A., Kienast, J.R., 2020. A case study of in situ analyses (major and trace elements, U-Pb geochronology and Hf-O isotopes) of a zircon megacryst: implication for the evolution of the Egéré terrane (Central Hoggar, Tuareg Shield, Algeria). Precambrian Res. 351, 105966. https://doi.org/10.1016/j.precamres.2020.105966.

Caddeo, G.A., de Waele, J., Frau, F., Bruce Railsback, L., 2011. Trace element and stable isotope data from a flowstone in a natural cave of the mining district of SW Sardinia (Italy): evidence for Zn^{2+}-induced aragonite precipitation in comparatively wet climatic conditions. Int. J. Speleol. 40, 181–190. https://doi.org/10.5038/1827-806X.40.2.10.

Cairncross, B., 2004. Field Guide to Rocks and Minerals of Southern Africa. Struik Publishers.

Chamberlin, G.J., Chamberlin, D.G., 1980. Colour, its Measurement, Computation, and Application. Heyden Int. Top. Sci.

Di Lorenzo, F., Ruiz-Agudo, C., Churakov, S.V., 2019. The key effects of polymorphism during PbII uptake by calcite and aragonite. CrystEngComm 21, 6145–6155. https://doi.org/10.1039/c9ce01040h.

Ding, W., Chen, Q., Li, Y., Liu, X., 2023. Origins of colour of Smithsonite from Yunnan, China. Minerals 13. https://doi.org/10.3390/min13020296.

Dutrizac, J.E., Chen, T.T., 1987. Mineralogical characterization of leach residues of a pyritic Zn-Pb-Cu-Ag concentrate. Can. Metall. Q. 26, 189–205. https://doi.org/10.1179/cmq.1987.26.3.189.

Fairchild, I.J., Smith, C.L., Baker, A., Fuller, L., Spötl, C., Mattey, D., McDermott, F., 2006. Modification and preservation of environmental signals in speleothems. Earth-Sci. Rev. 75, 105–153. https://doi.org/10.1016/j.earscirev.2005.08.003.

Faure, M., Charonnat, X., Chauvet, A., Chen, Y., Talbot, J.-Y., Martelet, G., Courrioux, G., Monie, P., Milesi, J.-P., 2001. Tectonic evolution of the Cevennes para-autochthonous domain of the Hercynian French Massif Central and its bearing on ore deposits formation. Bull. la Société Géologique Fr. https://doi.org/10.2113/172.6.687.

Gázquez, F., Calaforra, J.M., Rull, F., Forti, P., García-Casco, A., 2012. Organic matter of fossil origin in the amberine speleothems from El Soplao Cave (Cantabria, Northern Spain). Int. J. Speleol. 41, 113–123. https://doi.org/10.5038/1827-806X.41.1.12.

Gèze, B., Pellet, J., Paloc, H., Bambier, A., Roux, J., Senaud, G., 1980. Notice explicative de la feuille Florac à 1/50000. Bur. Rech. Géologiques Minières, Orléans, p. 52.

Günther, D., Heinrich, C.A., 1999. Enhanced sensitivity in laser ablation-ICP mass spectrometry using helium-argon mixtures as aerosol carrier. J. Anal. At. Spectrom. 14, 1363–1368. https://doi.org/10.1039/a901648a.

Hershey, O.S., Barton, H.A., 2018. The microbial diversity of caves. In: Cave Ecology, 69–90. Springer, Cham. https://doi.org/10.1007/978-3-319-98852-8_5.

Hitzman, M.W., Reynolds, N.A., Sangster, D.F., Allen, C.R., Carman, C.E., 2003. Classification, genesis, and exploration guides for nonsulfide zinc deposits. Econ. Geol. 98, 685–714. https://doi.org/10.2113/gsecongeo.98.4.685.

Joannopoulos, J.D., 2008. Photonic Crystals: Molding the Flow of Light, 2nd ed. Princeton University Press.

Judd, D.B., Wyszecki, G., 1975. Color in Business, Science and Industry. John Wiley Sons.

Lambiel, F., Dold, B., Spangenberg, J.E., Fontboté, L., 2023. Neoformation of exotic copper minerals from gel-like precursors at the Exótica deposit, Chuquicamata, Chile. Mineral. Deposita 58, 661–680. https://doi.org/10.1007/s00126-022-01148-6.

Maciejewska, M., Pessi, I.S., Arguelles-Arias, A., Noirfalise, P., Luis, G., Ongena, M., Barton, H., Carnol, M., Rigali, S., 2015. Streptomyces lunaelactis sp. nov., a novel ferroverdin A-producing Streptomyces species isolated from a moonmilk speleothem. Antonie van Leeuwenhoek. Int. J. Gen. Mol. Microbiol. 107, 519–531. https://doi.org/10.1007/s10482-014-0348-4.

Martín-García, R., Alonso-Zarza, A.M., Martín-Pérez, A., Schröder-Ritzrau, A., Ludwig, T., 2014. Relationships between colour and diagenesis in the aragonite-calcite speleothems in Basajaún Etxea cave. Spain. Sediment. Geol. 312, 63–75. https://doi.org/10.1016/j.sedgeo.2014.08.001.

Mondillo, N., Boni, M., Balassone, G., 2011. Supergene Zn-dolomite: an old-new actor on the nonsulphide ore scene. In: Geophysical Research Abstracts, p. 11958.

Moreau, J.D., Trincal, V., André, D., Baret, L., Jacquet, A., Wienin, M., 2018. Underground dinosaur tracksite inside a karst of southern France: early jurassic tridactyl traces from the dolomitic formation of the Malaval cave (Lozère). Int. J. Speleol. 47, 29–42. https://doi.org/10.5038/1827-806X.47.1.2149.

Mouchet, S.R., Deparis, O., 2021. Natural Photonics and Bioinspiration. Artech House.

O'Day, P.A., Carroll, S.A., Waychunas, G.A., 1998. Rock-water interactions controlling zinc, cadmium, and lead concentrations in surface waters and sediments, U.S. Tri-State Mining 1. Molecular identification using X-ray absorption spectroscopy. Environ. Sci. Technol. 32, 943–955. https://doi.org/10.1021/es970453c.

Pearce, N.J.G., Perkins, W.T., Westgate, J.A., Gorton, M.P., Jackson, S.E., Neal, C.R., Chenery, S.P., 1997. A compilation of new and published major and trace element data for NIST SRM 610 and NIST SRM 612 glass reference materials. Geostand. Newslett. 21, 115–144. https://doi.org/10.1111/j.1751-908X.1997.tb00538.x.

Perruchot, A., Dupuis, C., De Putter, T., Nicaise, D., Arbey, F., 2001. Paragenèses silico-alumineuses précoces d'âge Quaternaire en contexte cryptokarstique (Haute-Normandie, France); implications pour l'argilogenèse. Comptes Rendus l'Académie des Sci. - Ser. IIA - Earth Planet. Sci, 332, pp. 315–322. https://doi.org/10.1016/s1251-8050(01)01547-6.

Ploquin, A., Allée, P., Baron, S., Beaulieu, J. De, Carignan, J., Laurent, S., Carlier, C. Le, Veslud, D., Lavoie, M., Pulido, M., Ploquin, A., Allée, P., Baron, S., 2003. Medieval Lead Smelting on the Mont Lozère, Southern France, in: Archaeometallurgy in Europe: International Conference, pp. 635–644.

Ploquin, A., Allée, P., Bailly-Maître, M.-C., Baron, S., de Beaulieu, J.-L., Carignan, J., Laurent, S., Lavoie, M., Mahé Le Carlier, C., Paradis, S., Peytavin, J., Pulido, M., 2004. PCR – Le Plomb argentifère ancien du Mont Lozère (Lozère) - À la recherche des mines, des minerais et des ateliers, des paysages et des hommes. Archéosciences. Rev. d'archéométrie 34, 99–114. https://doi.org/10.4000/archeomed.53323.

Poot, J., Buelens, P., Dekoninck, A., Rochez, G., Yans, J., 2024. Tracing the Eh–pH evolution of Cu–Pb–As–Zn supergene mineralization using detailed petrography in the Cap Garonne mineral deposit (Provence, France). Mineral. Deposita. https://doi.org/10.1007/s00126-024-01258-3.

Prassl, J.-A., 1997. Exploitation antique dans le secteur minier du Bleymard (Lozère). Actes du Colloq. "Mines métallurgie la Préhistoire au Moyen-Age en Languedoc-Roussillon régions périphériques", pp. 217–224.

Samouhos, M., Zavašnik, J., Rečnik, A., Godelitsas, A., Chatzitheodoridis, E., Sanakis, Y., 2015. Spectroscopic and nanoscale characterization of blue-coloured smithsonite (ZnCO3) from Lavrion historical mines (Greece). Period. di Mineral. 84, 373–388. https://doi.org/10.2451/2015PM0019.

Skarpelis, N., Argyraki, A., 2009. Geology and origin of supergene ore at the lavrion Pb-Ag-Zn deposit, Attica. Greece. Resour. Geol. 59, 1–14. https://doi.org/10.1111/j.1751-3928.2008.00076.x.

Steinberg, M., Rautureau, M., Rivière, M., 1985. Analysis of zinciferous clays from central Tunisia using a scanning transmission electron microscope (STEM). Chem. Geol. 48, 157–164. https://doi.org/10.1016/0009-2541(85)90043-9.

Takahashi, T., 1960. Supergene alteration of zinc and lead deposits in limestone. Econ. Geol. 55, 1083–1115. https://doi.org/10.2113/gsecongeo.55.6.1083.

Tisato, N., Torriani, S.F.F., Monteux, S., Sauro, F., De Waele, J., Tavagna, M.L., D'Angeli, I.M., Chailloux, D., Renda, M., Eglinton, T.I., Bontognali, T.R.R., 2015. Microbial mediation of complex subterranean mineral structures. Nat. Sci. Rep. 5, 1–10. https://doi.org/10.1038/srep15525.

Turner, K., 2002. Chromophores Producing Blue Speleothems at Cliefden, NSW. Helictite, 38, pp. 3–6.

Van Achterberg, E., Ryan, C.G., Jackson, S.E., Griffin, W.L., 2001. Data reduction software for LA-ICP-MS: appendix. In: Sylvester, P.J. (Ed.), Laser Ablation-ICP-Mass Spectrometry in the Earth Sciences: Principles and Applications, pp. 239–243.

Verhaert, M., Bernard, A., Dekoninck, A., Lafforgue, L., Saddiqi, O., Yans, J., 2017. Mineralogical and geochemical characterization of supergene Cu–Pb–Zn–V ores in the Oriental High Atlas, Morocco. Mineral. Deposita 52, 1049–1068. https://doi.org/10.1007/s00126-017-0753-5.

Verheyden, S., 2004. Trace elements in speleothems. A short review of the state of the art. Int. J. Speleol. 33, 95–101. https://doi.org/10.5038/1827-806x.33.1.9.

Vlieghe, M., Rochez, G., Pire-Stevenne, S., Storme, J.Y., Dekoninck, A., Vanbrabant, Y., Namur, O., Zhang, Y., Van Ham-Meert, A., Donnadieu, J.P., Berbigé, M., Hasbroucq, J.L., Yans, J., 2023. Ni-rich mineral nepouite explains the exceptional green color of speleothems. Sci. Rep. 13, 1–8. https://doi.org/10.1038/s41598-023-41977-7.

White, W.B., 1997. Color of speleothems. In: Forti & Hill, Cave Minerals of the World, pp. 239–244.

White, W.B., 2019. Speleothems, 3rd ed. Elsevier Inc., Encyclopedia of Caves https://doi.org/10.1016/b978-0-12-814124-3.00117-5.

Zafiu, C., Part, F., Ehmoser, E.K., Kähkönen, M.A., 2021. Investigations on inhibitory effects of nickel and cobalt salts on the decolorization of textile dyes by the white rot fungus Phanerochaete velutina. Ecotoxicol. Environ. Saf. 215. https://doi.org/10.1016/j.ecoenv.2021.112093.